

AD-A103 735

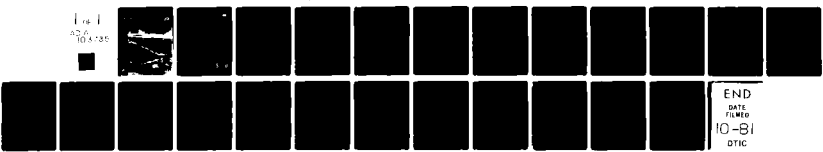
COLD REGIONS RESEARCH AND ENGINEERING LAB HANOVER NH F/G 20/14  
VHF ELECTRICAL PROPERTIES OF FROZEN GROUND NEAR POINT BARROW, A--ETC(U)  
JUN 81 S A ARNONE, A J DELANEY

UNCLASSIFIED

CRREL-81-13

NL

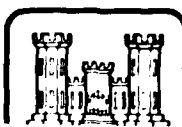
Fig 1  
42-6  
10-4-85



END  
DATE  
FILED  
10-81  
DTIC

# CRREL

## REPORT 81-13



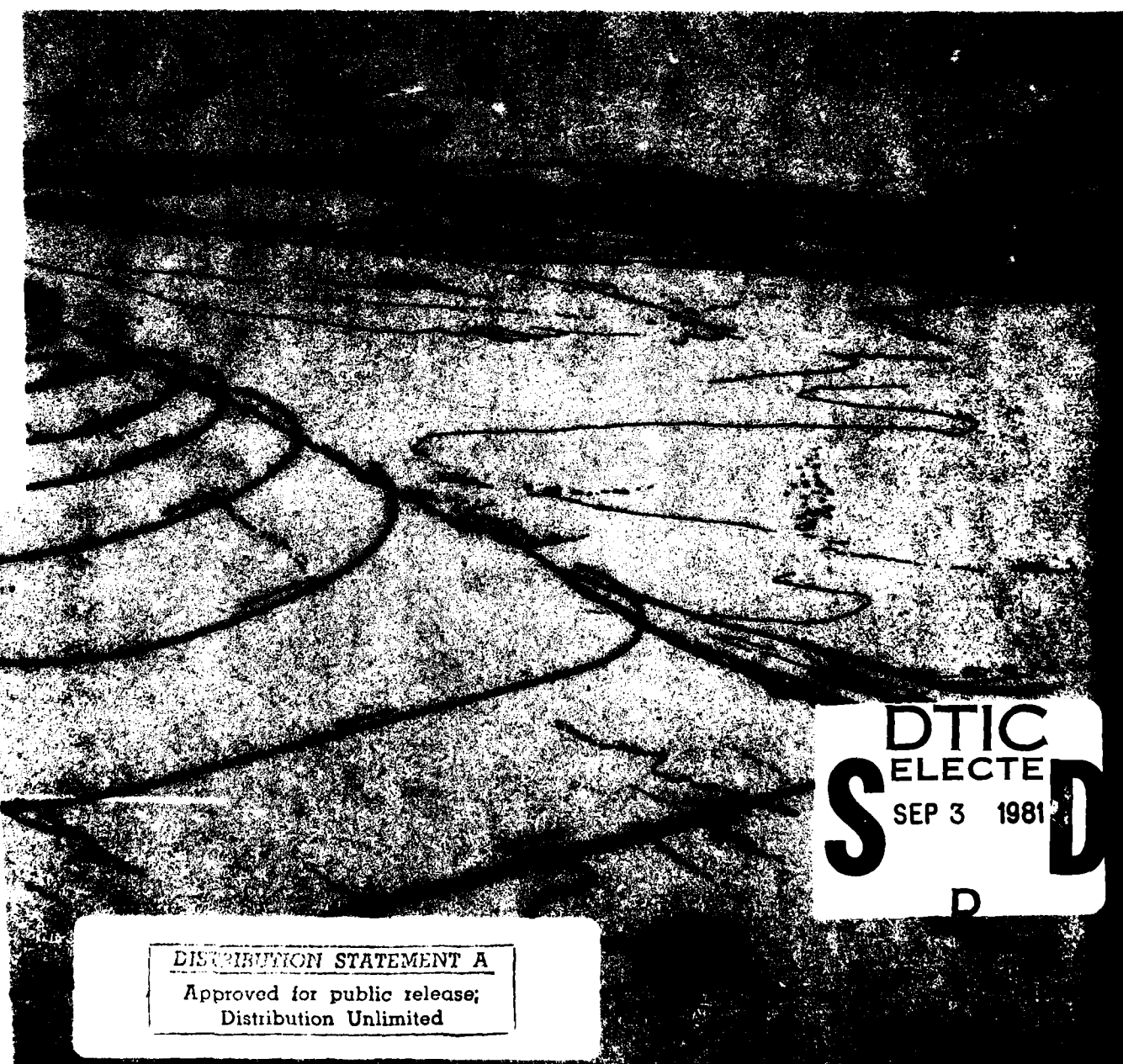
LEVEL II



VHF electrical properties of frozen ground  
near Point Barrow, Alaska

ADA103735

DTIC FILE COPY



DISTRIBUTION STATEMENT A  
Approved for public release;  
Distribution Unlimited

81 9 03.060

# CRREL Report 81-13



## *VHF electrical properties of frozen ground near Point Barrow, Alaska*

Steven A. Arcone and Allan J. Delaney

June 1981

Accession For	
NTIS GRA&1	
DTIC TAB	
Unannounced	
Justification	
By _____	
Distribution/ _____	
Availability Codes	
Dist	Avail and/or
	Special
A	

Prepared for  
DIRECTORATE OF MILITARY PROGRAMS  
OFFICE OF THE CHIEF OF ENGINEERS  
By  
UNITED STATES ARMY CORPS OF ENGINEERS  
COLD REGIONS RESEARCH AND ENGINEERING LABORATORY  
HANOVER, NEW HAMPSHIRE, U.S.A.

Approved for public release, distribution unlimited

DTIC  
ELECTE  
SEP 3 1981  
S D

Unclassified

SECURITY CLASSIFICATION OF THIS PAGE (When Data Entered)

REPORT DOCUMENTATION PAGE		READ INSTRUCTIONS BEFORE COMPLETING FORM
1. REPORT NUMBER CRREL Report 81-13	2. GOVT ACCESSION NO. AD-A103	3. RECIPIENT'S CATALOG NUMBER 735
4. TITLE (and Subtitle) VHF ELECTRICAL PROPERTIES OF FROZEN GROUND NEAR POINT BARROW, ALASKA	5. TYPE OF REPORT & PERIOD COVERED	
7. AUTHOR(s) Steven A. Arcone and Allan J. Delaney	6. PERFORMING ORG. REPORT NUMBER	
9. PERFORMING ORGANIZATION NAME AND ADDRESS U.S. Army Cold Regions Research and Engineering Laboratory Hanover, New Hampshire 03755	10. PROGRAM ELEMENT, PROJECT, TASK AREA & WORK UNIT NUMBERS DA Project/4A161102AT24 Task C/E1 Work Unit 005	
11. CONTROLLING OFFICE NAME AND ADDRESS Directorate of Military Programs Office of the Chief of Engineers Washington, D.C. 20314	12. REPORT DATE June 1981	
14. MONITORING AGENCY NAME & ADDRESS (if different from Controlling Office)	13. NUMBER OF PAGES 21	
16. DISTRIBUTION STATEMENT (of this Report) Approved for public release; distribution unlimited.	15. SECURITY CLASS. (of this report) Unclassified	
17. DISTRIBUTION STATEMENT (of the abstract entered in Block 20, if different from Report)	15a. DECLASSIFICATION/DOWNGRADING SCHEDULE	
18. SUPPLEMENTARY NOTES		
19. KEY WORDS (Continue on reverse side if necessary and identify by block number) Dielectric properties Permafrost Pt. Barrow, Alaska Radio interferometry		
20. ABSTRACT (Continue on reverse side if necessary and identify by block number) Electrical properties of frozen ground were measured using radio frequency interferometry (RFI) in the very high frequency (VHF) radiowave band. Ice-rich organic silts and sands and gravels of variable ice content were investigated during early April of both 1979 and 1980. Frequencies between 10 and 150 MHz were used with best results obtained between 40 and 100 MHz. Surface impedance and magnetic induction techniques were also used to obtain an independent measure of low frequency resistivity and to obtain a separate control on vertical inhomogeneity. Soil samples were tested for organic and water content. The dielectric constants determined for the ice-rich organic silts ranged from 4.0 to 5.5 while those for the sands and gravels were about 5.1. Dielectric loss was due to d.c. conduction and was very low for the silts but significant for the sands and gravels. The higher values for the sands and gravels		

Unclassified

SECURITY CLASSIFICATION OF THIS PAGE(When Data Entered)

20. Abstract (cont'd).

were most likely due to the higher concentrations of salt that are reported to exist in the old beach ridges in this region. All the RFI measurements are believed to be indicative of only the first few meters of the ground although the radiowaves could penetrate to tens of meters.

## PREFACE

This report was prepared by Dr. Steven A. Arcone, Geophysicist, and Allan J. Delaney, Physical Science Technician, of the Physical Sciences Branch, Research Division, U.S. Army Cold Regions Research and Engineering Laboratory. Funding for this research was provided by DA Project 4A161102AT24, *Research in Snow, Ice and Frozen Ground*, Task C/E1, *Cold Environment Factors*, Work Unit 005, *Dielectric Characteristics of Frozen Soils*.

The authors wish to thank Paul Sellmann and Donald Albert of CRREL for technically reviewing the manuscript of this report.

The contents of this report are not to be used for advertising or promotional purposes. Citation of brand names does not constitute an official endorsement or approval of the use of such commercial products.

## CONTENTS

	Page
Abstract .....	i
Preface .....	iii
Introduction.....	1
Background .....	1
Objectives and procedures .....	2
Theory and instrumentation.....	2
Radio frequency interferometry.....	2
Case 1: Homogeneous ground model.....	3
Case 2: Two-layer ground model .....	4
RFI instrumentation.....	5
Low frequency methods.....	6
Point Barrow sites .....	6
Results and discussion.....	8
Site 1: Tundra.....	8
Site 2: Beach ridge.....	10
Site 3: Marsh .....	11
Conclusions.....	13
Literature cited .....	14
Appendix A: Discussion of low-frequency geophysical methods .....	17

## ILLUSTRATIONS

### Figure

1. Radiation modes produced by a horizontal electric dipole antenna on the ground surface .....	3
2. Theoretical ground wave-air wave interference for two different values of $\tan\delta$ .....	4
3. Radiation modes produced by a horizontal electric dipole antenna on the surface of a two-layer ground model .....	4
4. Theoretical interference pattern of two surface waves matched to two cylindrical waveguide modes in the upper layer of a two-layer ground model.....	5
5. Schematic diagram of system used in radio frequency interferometry .....	6
6. Location map for the Pt. Barrow, Alaska, investigations.....	7
7. April 1979 RFI plots of four frequencies at site 1.....	8
8. April 1980 RFI plots at six frequencies at site 1.....	8
9. Magnetic induction and surface impedance data for site 1 during 1979 and 1980 .....	9
10. Illustration of the probable cause of the homogeneous behavior observed at site 1.....	9
11. April 1979 RFI profile at 88 MHz at site 2.....	10
12. April 1980 RFI profiles at six frequencies at site 2.....	10
13. Magnetic induction and surface impedance data for site 2 during 1979 and 1980 .....	11
14. RFI profiles at three frequencies for April 1979 at site 3.....	12
15. RFI profile at 88 MHz for April 1980 at site 3.....	12

# VHF ELECTRICAL PROPERTIES OF FROZEN GROUND NEAR POINT BARROW, ALASKA

Steven A. Arcone and Allan J. Delaney

## INTRODUCTION

### Background

Knowledge of the earth's electrical properties is important to many disciplines of science and engineering. This knowledge is used to interpret geologic strata, find concentrations of valuable minerals, determine geologic suitability for construction projects, predict radiowave propagation range, and for a host of other applications such as soil moisture detection and monitoring of water quality. In permafrost regions, the low electromagnetic (EM) absorption of frozen earth and the contrasting electrical properties of thawed soil, massive ice and frozen soil make electrical and EM methods suitable for subsurface exploration.

The most widely used electrical methods of permafrost exploration have been the direct current and the magnetic induction techniques, the latter employing loop antennas usually operating at 40 kHz and below. The depth of exploration of these methods strongly depends on electrode or antenna spacing so that subsurface detail is greatly sacrificed as depth of exploration is increased. Since 1970, however, detailed exploration of depths of up to 20 m in soils has become possible with the advance of short-pulse ground radar, originally pioneered during the 1960's for radio glaciology studies. Just as radio glaciology spurred many efforts to determine the dielectric properties of glacial ice, so have permafrost radar studies stimulated efforts to determine the dielectric properties of frozen soils and rocks.

This report presents the results of field studies of permafrost dielectric properties within the very high frequency band (VHF, 30 to 300 MHz) currently used in subsurface radar. This frequency range is ideal for subsurface radar because absorption due to free pore water is minimized for many earth materials. However, the permanent dipole moment of the water molecule adsorbed on particle surfaces can strongly affect dielectric properties in this range, as has been shown by Hoekstra and Doyle (1971), Hasted (1973) and Olhoeft (1977).

The electrical properties of interest are  $\kappa'$  and  $\kappa''$ , the real and imaginary parts, respectively, of the relative complex permittivity which determines the index of refraction  $n$ . When  $\kappa''/\kappa' < 0.1$ ,  $\kappa'$  determines the velocity of propagation and  $\kappa''$  the wave absorption. The quantity  $\kappa''$  is determined by conductive (or ohmic) and dielectric relaxation losses, neither of which can be separated in a single measurement. Therefore, dielectric measurements are usually presented as the real permittivity  $\kappa'$  (most commonly called the "dielectric constant") and the ratio  $\kappa''/\kappa' = \tan \delta$  (the loss tangent).

Olhoeft (1977) and Katsube et al. (1976) used bridge impedance techniques to study frozen clay to about 10<sup>6</sup> Hz and have measured  $\kappa' = 0.3$  at -10°C. Olhoeft estimated that this value of  $\kappa'$  should remain constant over at least another frequency decade while  $\tan \delta$  will trend toward a minimum between 10<sup>8</sup> and 10<sup>9</sup> Hz. Observations at higher frequencies using waveguide and time domain reflectometry (TDR) measurements were reported by Hoekstra and Delaney

(1974). Their data showed greatest dispersion at a relaxation frequency of about 1 GHz for a 10% water (by weight) clay. Hoekstra and Delaney also investigated a silty clay at frequencies as low as 100 MHz, where they found similar results at a water content of 10% by weight. Frozen silts, the primary material encountered in our study, have not been investigated as extensively as clays, although dielectric values for dry silt at 500 MHz were reported by Hoekstra and Delaney (1974). They found  $\kappa'$  values of approximately 3 for Fairbanks silt and also for a silty clay, pure clay (engineering classification), and a fine sand, all at zero water content.

The above measurements of  $\kappa'$  and  $\kappa''$  were all performed at  $-10^{\circ}\text{C}$ , a temperature at which some adsorbed water is known to remain in the soil/ice matrix. When temperature is depressed even further, the freezing of any remaining adsorbed water will lower  $\kappa'$  for a soil to usually between 3 and 5 and  $\tan \delta$  to 0.01 or less. These values are consistent with the dielectric constant values of between 3 and 5 for ice and dry soils as have been reported by Von Hippel (1954), Cook (1960) and Hoekstra and Delaney (1974).

Field measurements of dielectric properties of permafrost near about 100 MHz have been carried out mainly by Canadian researchers at the Involted Hill test site in Tuktoyaktuk, N.W.T., using impulse radar and antenna impedance techniques. The impulse radar method was used by Davis et al. (1976), and Annan and Davis (1976) discussed the use of impulse radar for wide angle reflection and refraction (WARR) sounding, which is similar procedurally to the techniques used in seismic prospecting. For ice-rich clay till, Annan and Davis (1976) measured  $\kappa'$  values between 2.5 and 4.2, the low end of which could not be justified by laboratory measurements of density and fractional air volume (Annan 1976). Wong et al. (1977) used a monopole inserted into the active layer to determine electrical properties from the antenna impedance. At 100 MHz in late winter,  $\kappa'$  was between 3 and 7 and resistivity at about  $10^4$  ohm-m for a frozen, very cold composite of peat, silt and clay till.

The method used in our investigation is known as radio frequency interferometry (RFI) which was described in detail by Annan (1973) and Rossiter et al. (1973). This method allows calculation of dielectric properties from the interference pattern of surface and ground wave modes propagated from an antenna lying on the ground surface. The method has been used in lunar (Strangway 1969) and glacial (Strangway et al. 1974) studies. Its first reported use in permafrost studies was by Rossiter et al. (1978) in the Tuktoyaktuk study area mentioned above. During winter at this site, a dielectric constant of 6 and an electrical

resistivity of about 2000 ohm-m were determined from a marginal interference pattern at 16 MHz for the ice-rich clay till. The resistivity value was thought to be entirely due to d.c. effects.

### Objectives and procedures

The objective of our research was to measure in situ the complex dielectric properties of very cold permafrost of various soil types at frequencies between about 50 and 150 MHz. We chose the RFI technique over impulse radar, antenna impedance and a variety of other waveguide insertion techniques for the following reasons:

1. Single frequencies could be investigated.
2. Depths to several meters might be realized if strong contrasts in dielectric properties existed at depth.
3. RFI does not require the ground to be disturbed by drilling and emplacement of metal structures.

In addition to the RFI technique, surface impedance and magnetic induction methods were used to measure low frequency resistivity and thus to compare it with high frequency resistivity values obtained from the attenuation of the interference patterns. The magnetic induction method was capable of being used in modes which allowed two separate penetration depths of approximately 3 and 7 m.

## THEORY AND INSTRUMENTATION

### Radio frequency interferometry

An antenna placed at or near the ground surface can excite several different modes of propagation as it radiates. These modes all propagate at different velocities, depending on whether they travel in air, in ground or through the ground by multiple subsurface reflections. If the antenna continuously radiates at a fixed frequency, these modes will combine along the surface to produce a standing wave interference pattern. The electrical and geometric (i.e. layer depth) properties of the ground may then be deduced from the separation of the interference fringes and the general attenuation rates for patterns of different frequencies.

The theory of ground wave propagation from a radiating source above a conductive earth was first presented by Sommerfeld (1909). Several theorists later made important contributions and refinements, with Norton (1937) finally giving the most complete analysis in a form that has been extensively used since. Wait (1951) considered an earth model for which conduction currents were less important than displacement currents, i.e. a very resistive earth. Wait's analysis was then elaborated upon by Annan (1973) who also calculated the radiated field above a layered earth for several antenna types. The ensuing discussion is based on

Annan's work with the electric field formulas developed from his theory. In this study, we deal only with electric dipole antennas lying horizontally on the ground surface and radiating continuously at a single frequency. Therefore, the theory discussed refers only to steady state solutions.

#### Case 1: Homogeneous ground model

An antenna placed on the ground surface can be shown to excite four distinct radiation modes. These modes are illustrated in Figure 1 which is referenced by a right-hand Cartesian coordinate system  $x, y, z$ . In this figure, wavefront A represents a spherical air wave above the surface, and wave B represents a spherical wave excited in the ground. Waves C and D propagate above and below the ground, respectively, in order to maintain the continuity of the tangential electric and magnetic fields of waves B and A across the air/ground interface. Wave C is termed "inhomogeneous" in that it attenuates exponentially with height above the surface. It propagates with the same phase velocity as B. Wave D is called a head wave and it propagates with the same horizontal phase velocity as A. The RFI technique utilizes the interference between waves C and A.

The velocity of wave propagation in the ground is much slower than in air. Consequently, in order for A to match D at the air/ground interface, the horizontal phase velocity of waves A and D must be equal. This forces wave D to propagate at an angle  $\beta$  such that  $\sin\beta = k_0/k_1$  where  $k_0$  and  $k_1$  are the propagation functions in air and ground respectively. They are given as

$$k_0 = \sqrt{\omega^2 \mu_0 \epsilon_0} \quad (1)$$

and

$$k_1 = \sqrt{\omega^2 \mu_0 \kappa^* \epsilon_0 + i \omega \mu_0 / \rho} \quad (2)$$

or

$$k_1 = k_0 \sqrt{\kappa' + i \kappa' \tan \delta} \quad (3)$$

where  $\tan \delta = (\kappa'' + 1/\rho \omega \epsilon_0)/\kappa'$ . In these expressions  $\omega$  is frequency in radians per second,  $\mu_0 = 4\pi \times 10^{-7}$  H/m,  $\epsilon_0 = 8.85 \times 10^{-12}$  F/m,  $\rho$  is resistivity in ohm-m and  $i = \sqrt{-1}$ .  $\kappa^*$  is the relative complex dielectric permittivity composed of real part  $\kappa'$  and imaginary part  $\kappa''$ . A time dependence of  $e^{-i\omega t}$  has been assumed.

Of particular interest is the horizontal electric field component  $E_x$  of the vector addition of waves A and C. This addition produces the sought-after above-surface interference pattern. The variation of  $E_x$  as a function of  $y$ , the direction perpendicular to the

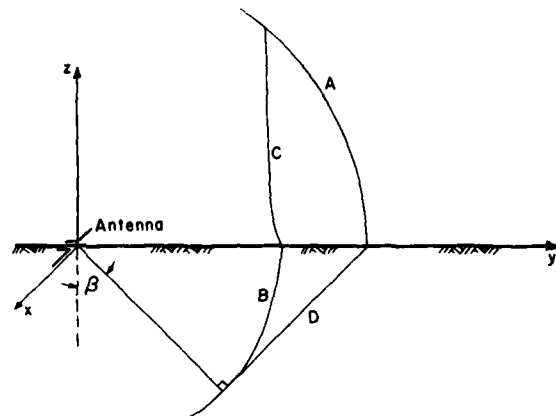


Figure 1. Radiation modes produced by a horizontal electric dipole antenna on the ground surface. A and B represent spherical wavefronts and D is a planar, refracted wavefront. Mode C represents an inhomogeneous wave that attenuates exponentially with height. The angle  $\beta = \sin^{-1}(k_0/k_1)$ . Figure adapted from Annan (1973).

antenna axis where  $x = z = 0$ , is found to be

$$E_x = \frac{2ik_0^2}{k_1^2 - k_0^2} \left( \frac{k_0 e^{ik_0 y}}{y^2} - \frac{k_1 e^{ik_1 y}}{y^2} \right) \quad (4)$$

+ terms of order  $1/y^3$  and  $1/y^4$ .

The first term in the parentheses describes wave A and the second term wave C. Beyond a distance of about one wavelength from the origin (source) the higher order terms may be neglected in comparison with the terms involving  $1/y^2$ .

Equation 4 shows the two waves A and C of Figure 1 to be propagating with a spatial attenuation rate proportional to  $1/y^2$ . In addition, there will also be attenuation due to any dielectric or conductive loss.

Two examples of ground and air interference at 100 MHz are shown in Figure 2. Both ground models are given a  $\kappa'$  value of 5 but with different values of  $\tan \delta$ . In both cases the value of  $\kappa'$  may be deduced from the formula

$$\kappa' = \left( \frac{\lambda_0}{\lambda_b} + 1 \right)^2 \quad (5)$$

as discussed by Rossiter et al. (1973), where  $\lambda_0$  is the free space wavelength and  $\lambda_b$  is the distance between interference minima. The value of  $\tan \delta$  can only be estimated qualitatively from the pattern, but a more quantitative estimate can be made by comparing the curves to theoretical models with  $\kappa'$  held at the measured value. Both curves in Figure 2 show a  $1/y^2$  envelope for the interference fringes beyond about 1-m range.

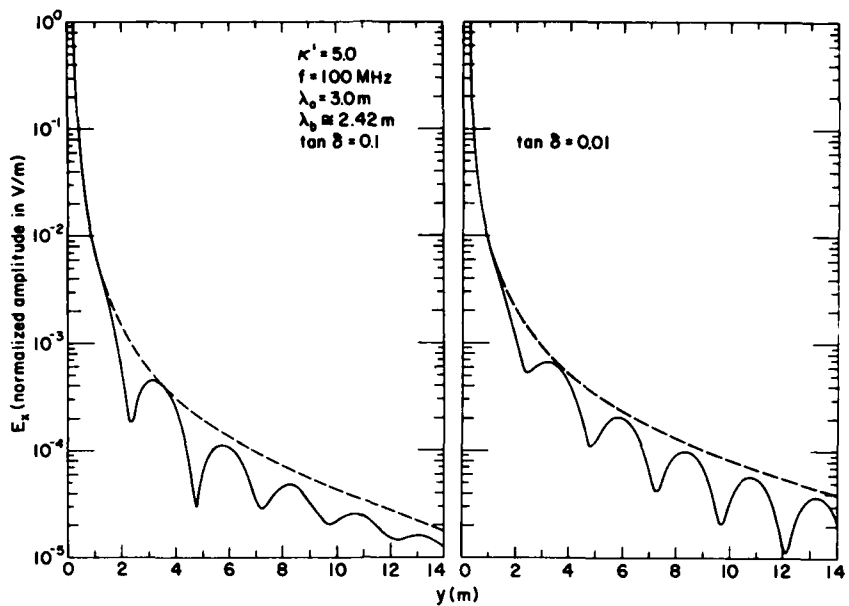


Figure 2. Theoretical ground wave-air wave interference for two different values of  $\tan \delta$ . The broken curves are  $1/y^2$  envelopes for  $\tan \delta = 0.0$ .

Deeper minima occur at larger ranges for lesser values of  $\tan \delta$ . The  $1/y^2$  attenuation rate is an important point for differentiating a homogeneous case from one that is layered. Layered models may often have a much lower rate of attenuation due to the entrainment of energy within the layers.

#### Case 2: Two-layer ground model

The addition of a subsurface interface may allow several additional modes to propagate and contribute to the surface field strength. These modes are illustrated in Figure 3. Wave A is the spherical air wave

and is matched by wave D as in case 1. In this case, however, wave D may reflect off the subsurface interface to give a more complex amplitude to wave A than in case 1. Waves  $B_1, B_2, \dots$ , etc., are a series of cylindrical modes within the upper layer which will be matched at the surface by a series of inhomogeneous cylindrical waves  $C_1, C_2, \dots$ , etc., propagating at the same horizontal phase velocities as  $B_1, B_2, \dots$ , etc. E is shown as a particular ray of the initial upper layer excitation that refracts along the subsurface interface with horizontal phase velocity  $\omega/k_2$ . This refraction along the subsurface interface will only occur if  $k_2 < k_1$ ; otherwise

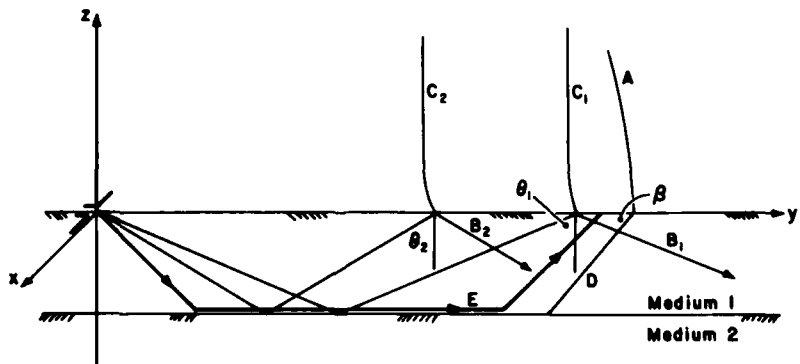


Figure 3. Radiation modes produced by a horizontal electric dipole antenna on the surface of a two-layer ground model. The addition of a second interface has caused wave B of Figure 1 to break into distinct modes (rays  $B_1, B_2, \dots$ ) some of which may strongly attenuate with distance. Curves A and D are phase fronts,  $B_1, B_2$  and E are ray normals.  $C_1$  and  $C_2$  indicate amplitude attenuation rates for the surface inhomogeneous waves. Here  $\beta$  is the complement of the angle of incidence of phase front D upon the lower interface.

wave E just refracts downward into the lower layer. The most important components in an interference pattern usually are the cylindrical modes which attenuate only as  $1/y^{1/2}$ . If two or more of these modes are strongly excited (i.e. little attenuation), then they will produce a strong interference pattern for considerably greater distances than occur for case 1.

Under ordinary circumstances, wave D cannot excite a refracted wave that would propagate along the subsurface interface because the angle of incidence  $\beta$  of wave D is determined by the contrast in properties between the air and the upper ground layer. In order to generate a refracted subsurface boundary wave there must be a similar contrast between layer 2 and layer 1. This requires layer 2 to have the dielectric properties of air, which is not a very common situation.

Mathematically, the two-layer solution for  $E_x$  from a point source horizontal electric dipole when  $z = x = 0$  can be expressed as

$$E_x = A(\theta_{10}^c) \frac{e^{ik_0 y}}{y^2} + \sum_i C_i(\theta_i) \frac{e^{ik_1 \sin \theta_i y}}{y^{1/2}} + E(\theta_{12}^c) [1 - b(\theta_{12}^c) y]^{-3/2} \frac{e^{ik_2 y}}{y^2} + H(1/y). \quad (6)$$

The quantity  $H(1/y)$  represents higher order terms in inverse powers of  $y$  which contribute negligibly to  $E_x$  beyond about one wavelength from the source. Terms  $A$ ,  $E$  and  $b$  are constants that depend on the critical angles of propagation, and  $\theta_{10}^c = \sin^{-1}(k_0/k_1)$  and

$\theta_{12}^c = \sin^{-1}(k_1/k_2)$ . Terms  $C_i$  are the constants for the dominant modes which propagate at the angles  $\theta_i$ . These angles are determined by solving the transcendental normal mode equation,

$$1 - R_{10}(\theta_i) R_{12}(\theta_i) e^{2/k_1 d \cos \theta_i} = 0, \quad (7)$$

for  $\theta_i$  where  $R_{10}$  and  $R_{12}$  are the interface reflection coefficients as seen from within the upper layer. This equation is an essential condition for forming a waveguide mode and is discussed in detail by Budden (1961).

If a two-layer ground condition is suspected, a series of theoretical curves must be generated for comparison with the observed data to determine the ground electrical properties. This can be a very cumbersome procedure even for just two layers. A simple case is presented in Figure 4 of a lossless dielectric situated above a perfect reflector. Only two guided modes are excited for this particular combination of dielectric constant and layer thickness, and a  $1/y^{1/2}$  attenuation rate begins within a few wavelengths from the source. When more modes are excited, energy can be focused at a particular range, thereby producing amplitude growth over small distances.

#### RFI instrumentation

Our implementation of the RFI method was extremely simple. Two dipole antennas were laid upon the ground parallel to each other, one for transmission and the other for reception. The antennas were then incrementally or continuously moved apart along a line perpendicular to the dipole axis and the received field strength was recorded as a function of position.

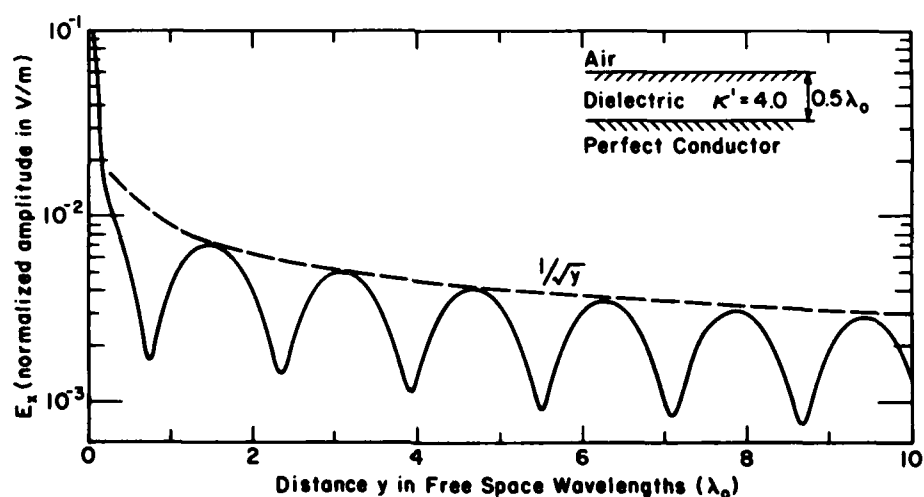


Figure 4. Theoretical interference pattern of two surface waves matched to two cylindrical waveguide modes in the upper layer of the two-layer ground model shown above. The curve is valid for  $\tan \delta < 0.001$ .

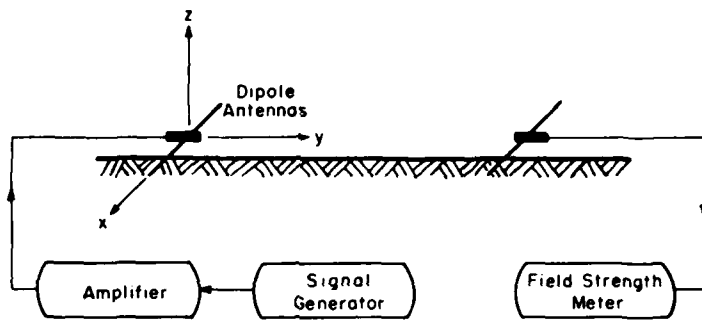


Figure 5. Schematic diagram of system used in radio frequency interferometry. The dipole antennas rest on the ground.

The components used in our investigations are shown schematically in Figure 5 with the antenna orientation shown relative to the coordinate system used in the theoretical development.

A Hewlett-Packard signal generator (model 8654A) supplied the VHF signal to a 10-W linear amplifier (Instruments for Industry Corp. model 5100). The amplified signal was fed to and transmitted from a tuned, half-wave resonant dipole. The received signal was detected with an identical tuned dipole and displayed on a high-sensitivity, high-frequency oscilloscope (Tektronix 475). All of the system cabling consisted of low loss, multi-shield, 75-ohm coaxial cable. A tuned RF voltmeter acquired for this project failed during both field seasons. The loss of this item probably allowed considerable interference in much of our data recorded at frequencies of 40 MHz and below.

In the field, two major deviations from the theory are the lateral inhomogeneity in the ground and the use of resonant half-wave dipoles instead of point sources. Lateral inhomogeneity is unavoidable but was probably not significant in our investigations. The use of half-wave dipoles enabled us to record data at antenna separations of over 40 m. The variation of  $E_x$  with range along the principal radiation direction of the antenna using a half-wave dipole deviates from that of a point source only within a few wavelengths of the antenna.

When expressed in their full form, the solutions for the inhomogeneous C waves describe exponential attenuation with height above ground. In our investigations, snow cover was usually about 20 to 30 cm and may have been a factor as discussed below.

#### Low frequency methods

Two other geophysical methods of investigation were used for the purposes of measuring ground resistivity and the presence of any near-surface stratification. These methods are known as the surface impedance (SI) and magnetic induction (MI) techniques

and are methods which respond mainly to the d.c. conductivity of the ground. Dielectric loss at frequencies in the VHF range may be due to both d.c. conduction and dielectric relaxation. Therefore, the use of these techniques allowed us to compare any measured ground resistivity using RFI with that of SI and MI.

The SI technique measures ground resistivity by comparing electromagnetic field components of a plane wave propagating from a distant transmitter usually in commercial or military use. The MI technique measures ground resistivity by comparing a secondary, induced magnetic field with the primary inducing field. Both methods operate within the VLF to LF range (15 to 400 kHz). They have been discussed extensively by Arcone (1979), Arcone et al. (1979) and Arcone and Delaney (1980) and are briefly reviewed in Appendix A.

#### POINT BARROW SITES

The locations of the sites studied near Pt. Barrow are shown in Figure 6. The near-surface sediments are composed of two major lithologic units described by Black (1964) and Sellmann and Brown (1973). Marine sediments known as the Barrow unit exist to an approximate depth of 7 m under our sites beneath which are marine sediments of the Skull Cliff unit. The Barrow unit can be subdivided into an uppermost layer of organic- and ice-rich silty sediments that have been highly reworked, and a lower, well-sorted sandy portion. The Skull Cliff unit consists largely of silts and sandy silts. A beach ridge borders the area marked as "marsh" in Figure 6 and presents most of the topographic relief in the area. The beach ridge is composed of sands and gravels reaching thicknesses up to 5 m.

Brown (1969) has shown salt concentrations to be increasing with depth beneath all the shallow sediments studied in this area. Our data obtained with low frequency resistivity methods are consistent with Brown's

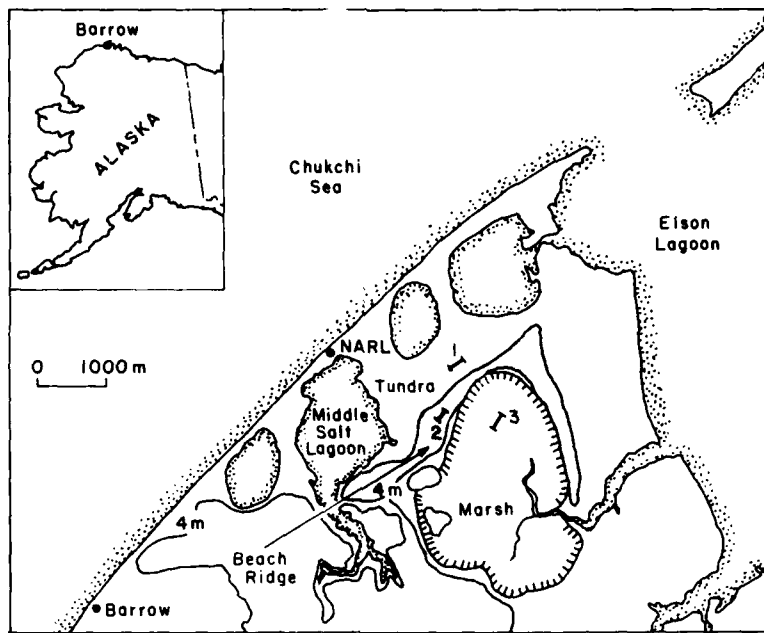


Figure 6. Location map for the Pt. Barrow, Alaska, investigations. Shaded area shows extent of the beach ridge.

observations in that ground resistivity decreases rapidly with depth throughout the area.

In the vicinity of our measurements, O'Sullivan (1963) has obtained conductivity vs depth profiles at several sites. His data reveal thin layers of such high conductivity (i.e. 1 ohm-m or less) that they are most probably composed of thawed brine. The depths of these layers were found to be as shallow as about 1.5 m but were usually greater than 2 m. It will be seen that this phenomenon verifies the unusual interpretation of some of our data.

The specific sites we investigated are marked 1, 2 and 3 in Figure 6. Data were obtained in late March and early April of 1979 and 1980 when the ground surface temperature (beneath the snowpack) was approximately  $-20^{\circ}\text{C}$ . The ground at this time for both years was covered with between 20 and 30 cm of hard-packed snow, except at site 2 where the snowcover was largely removed due to its higher elevation. Data were collected along linear traverses, one at each site, of up to 40 m length. At three locations along each traverse, soil samples were collected to approximately 1-m depth.

The names given our sites in Figure 6 describe the landform upon which they occur. Site 1 (tundra) was well-drained with the soils containing large quantities of ground ice. The soil samples from this site showed the greatest range and highest values for water content of all three sites, ranging between 1.33 and 12.65

grams water/gram soil. The soil samples nearest the surface also had the highest range of organic content with values ranging between 24 and 69% of dry weight. Site 2 (beach ridge) had the best surface drainage. The water content of the near-surface samples ranged between 0.37 and 1.38 grams water/gram soil, with organic content ranging between 2.8% and 19% of dry weight. Site 3 (marsh) was a wet site with poor summer surface drainage that had approximately 20 cm of pond ice overlying the soil. The soil samples had water contents of approximately 1.20 to 3.80 grams water/gram soil with organic content ranging between 12 and 28% of dry weight.

Subsurface temperature profiles were not made but are available in the literature (Lachenbruch 1973, Brown and Johnson 1965) for the Barrow area. Temperatures within 1 m of the surface can be as low as  $-30^{\circ}\text{C}$  by early April. Generally, however, temperature drops to  $-12^{\circ}\text{C}$  after the first few meters and then increases at less than  $2^{\circ}\text{C}$  per 100 m of depth. The active layer at Pt. Barrow seldom exceeds 30 cm in depth. The soil samples taken from below this depth showed no significant change in water content but the organic content did generally decrease with depth.

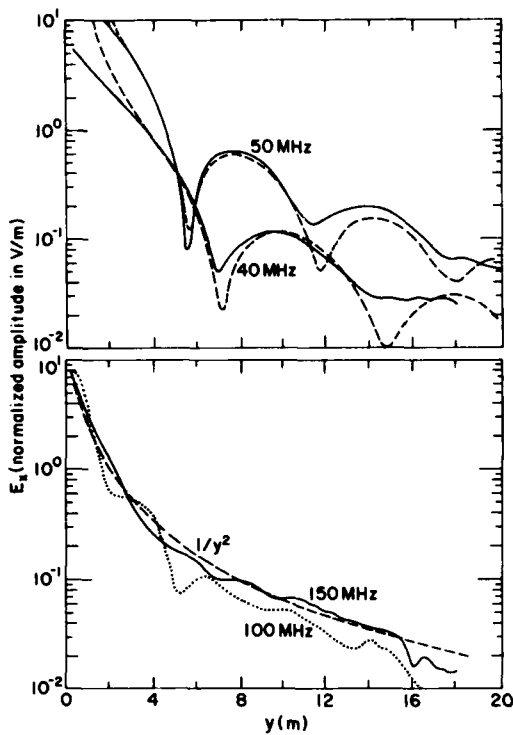


Figure 7. April 1979 RFI plots of four frequencies at site 1. Broken lines in top curve are theoretical for  $\kappa' = 4.0$ ,  $\rho = 4500 \text{ ohm-m}$ .

## RESULTS AND DISCUSSION

In this section both RFI and low frequency resistivity data taken in April of 1979 and 1980 are presented for each of the three sites. At frequencies of 80 MHz and above, readings were made every  $1/3$  m and below 80 MHz every  $1/2$  m. In many cases data were extremely poor; however, excellent RFI interference patterns were obtained for at least one frequency (generally between 40 and 100 MHz) at each site. The lack of a tuned receiver and the existence of a snow cover prevented widening this band to the general range of 10 to 250 MHz in which the rest of our system was capable of operating.

### Site 1. Tundra

The RFI profiles performed in 1979 and 1980 are given in Figures 7 and 8. The 40- and 50-MHz data in Figure 7 compare well with a homogeneous model earth of  $\kappa' = 4.0$  and  $\rho = 4500 \text{ ohm-m}$ , values which give an effective  $\kappa'' = 0.08$  at 50 MHz. The nulls are not well-pronounced in the 100-MHz profile in Figure 7; but their spacing again indicates that  $\kappa' = 4.0$  using eq 5. The 150-MHz profile in Figure 7 shows practi-

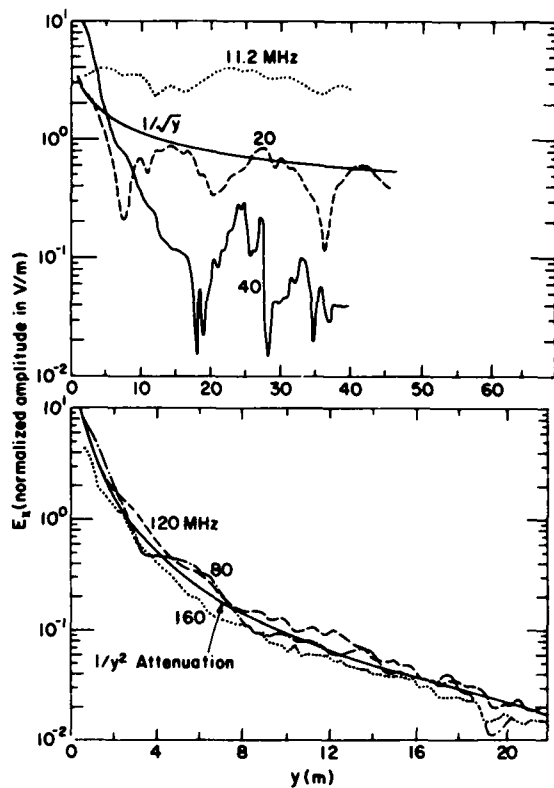


Figure 8. April 1980 RFI plots at six frequencies at site 1.

cally no nulls, and ordinarily this would indicate very low resistivity. However, the attenuation of the ground wave signal strength with height above the earth's surface is proportional to  $\exp[-(k_1^2 - k_0^2)^{1/2} z]$  which, in this case, gives nearly a 10-dB attenuation per 20 cm of height. Since the snowpack was at least of this depth, the absence of interference at this high frequency is expected.

The 1980 data at site 1 are shown in Figure 8. In 1980 we attempted to take data down to 11.2 MHz, whereas during 1979 severe interference from a local transmitter limited our lowest frequency to 40 MHz. The lower set of traces in Figure 8 (for 80 MHz and above) show characteristic  $1/y^2$  attenuation but do not contain an interpretable interference pattern, while the upper traces of Figure 8 show that external interference was still prevalent. The profile at 20 MHz shows an attenuation characteristic of a  $1/y^{1/2}$  dependency, which might suggest that a strongly conducting interface existed at depth. However, these data cannot be modeled because they extend over a range of only about three free space wavelengths at 20 MHz (the range was limited by available cable length). This allowed us only about one wavelength of range in

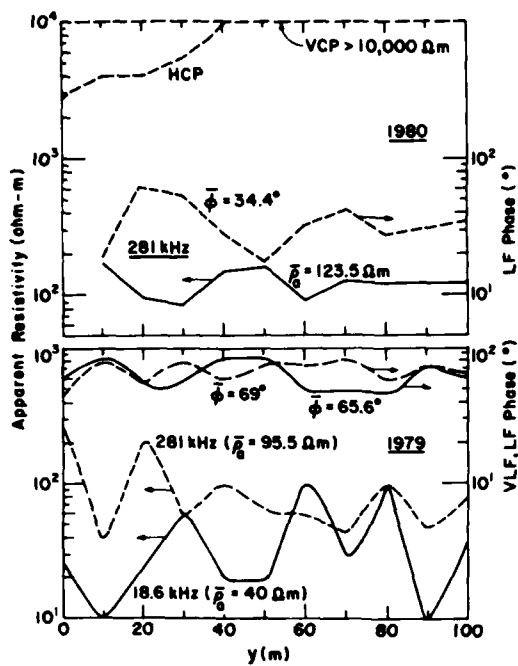


Figure 9. Magnetic induction and surface impedance data for site 1 during 1979 and 1980. Upper plots on top graph are magnetic induction readings in ohm-m of apparent resistivity. For 1979 data, all magnetic induction readings are  $> 10,000$  ohm-m. Arrows refer to applicable scales.

which our measurements could be modeled. The 11.2-MHz data of Figure 8 extended only about 1.5 wavelengths and showed no decay with distance. The quality of the data at 40 MHz contrasts sharply with that from 1979 and could not be interpreted due to its erratic behavior. Although nulls are present, none appear within the first 16 m as they did in 1979.

The results of the low frequency geophysical investigations for 1979 and 1980 are shown in Figure 9. The MI data for both years indicated that ground resistivity was greater than 10,000 ohm-m to a depth of at least two to three intercoil spacings (7 to 11 m), while the 1979 SI phase data indicated that resistivity was decreasing with depth because values were consistently greater than 45°. This conclusion is entirely plausible but contradicts the 40-MHz RFI data that imply electrical homogeneity to at least a skin depth. At 40 MHz, with  $\kappa' = 4$  and  $\rho = 4500$  ohm-m, the skin depth would be about 50 m, a depth for which homogeneity is impossible due to increases of salt concentration.

This contradiction is resolved, however, by an explanation illustrated in Figure 10. In this figure, hypothetical subsurface wavefronts are shown as continually obliterating from ideal spherical wavefronts (for a homogeneous case) while their associated ray normals

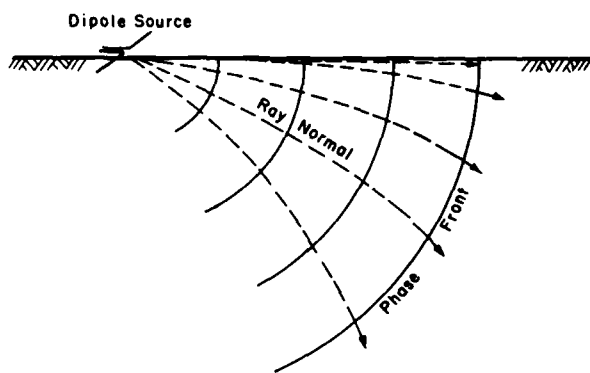


Figure 10. Illustration of the probable cause of the homogeneous behavior observed at site 1. The refractive index continuously increases with depth causing the ray normals to bend downwards. Therefore, no strong subsurface reflections occur to disturb the  $1/y^2$  attenuation rate of the wavefronts just below the surface.

bend toward the vertical. This behavior would be the response to an increase of salt concentration with depth which also would cause resistivity and  $n$ , the index of refraction, to increase with depth. Since no sharp interfaces exist, no deviation from the  $1/y^2$  homogeneous attenuation behavior would be observed at the surface where the subsurface wavefronts remain evenly spaced with distance.

Major inconsistencies are to be found in the SI data itself. In 1979 phases were well above 45°, reflecting the decrease of resistivity with depth, whereas in 1980 the phase at 281 kHz averaged below 45° and was not consistent with the resistivity profiles. This contrast in phase data between the two years occurred at all sites and is believed to result from an instrument calibration error. In addition, the amplitude of the SI data was extremely low for both years, giving average apparent resistivity ( $\rho_a$ ) values of about 100 ohm-m at 281 kHz and 40 ohm-m at 18.6 kHz. If one assumes that at least the top 7 m is at 5000 to 10,000 ohm-m, then within just a few more meters, resistivity would have to drop to 5 to 10 ohm-m to generate the 1979 data observed. If such a decrease did occur, the MI values would have to be much lower.

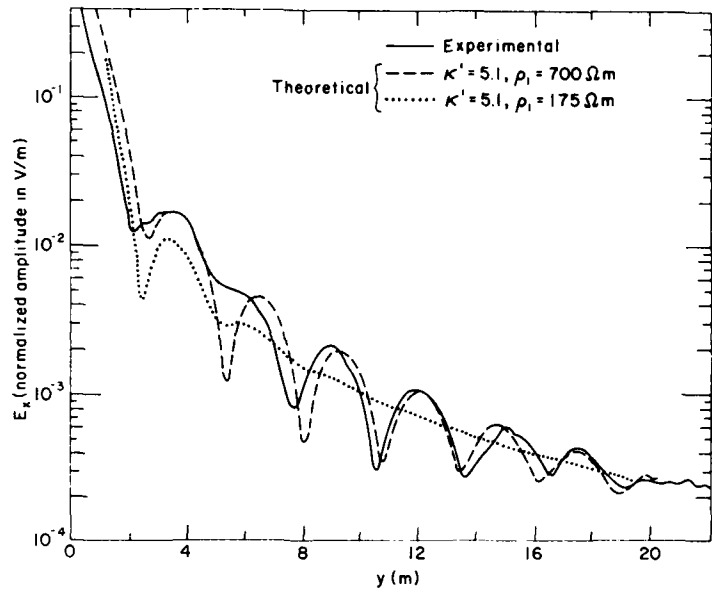


Figure 11. April 1979 RFI profile at 88 MHz at site 2.

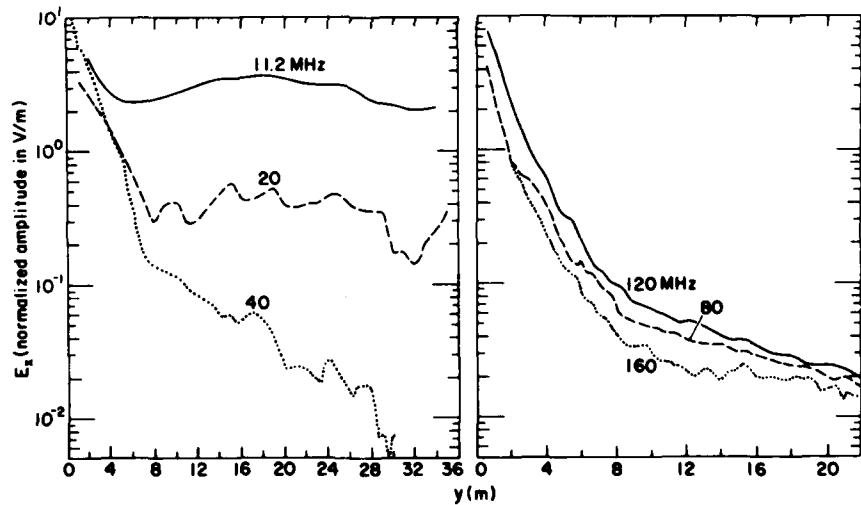


Figure 12. April 1980 RFI profiles at six frequencies at site 2.

#### Site 2, beach ridge

The RFI profiles performed in 1979 and 1980 are given in Figures 11 and 12 respectively. The data were taken over nearly barren ground, as the snow cover was marginal over this ridge. Only one frequency (88 MHz) was investigated in 1979. In 1980, however, the data obtained were erratic and similar to those obtained at site 1 during 1980. At 80 MHz and above (Fig. 12)

the attenuation rate was clearly  $1/y^2$  while at 40 MHz and below almost no similarity to any attenuation function was observed.

Model electrical parameters chosen for generating theoretical curves to fit the data of Figure 11 were chosen from the null spacing of the data and also from the resistivity values measured with the MI technique (Fig. 13) which were consistent for both years.

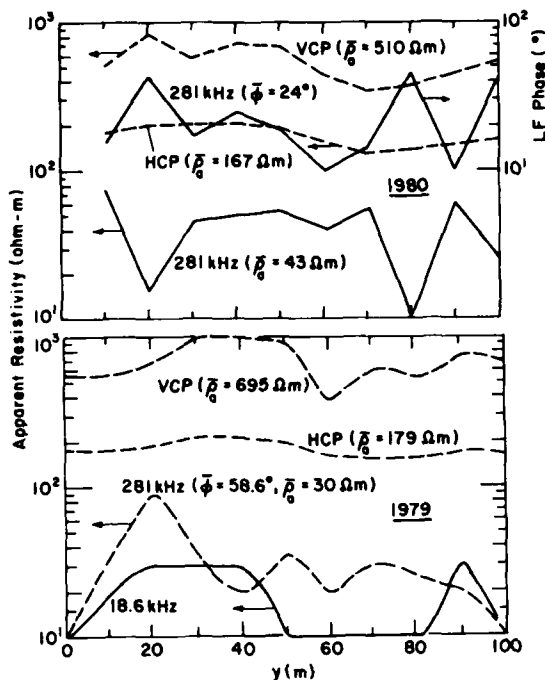


Figure 13. Magnetic induction and surface impedance data for site 2 during 1979 and 1980. Upper plots on each graph are magnetic induction readings in ohm-m of apparent resistivity. Average surface impedance phase for 1979 given in parentheses. Arrows refer to applicable scales.

The average null spacing in the data gave a dielectric constant of 5.1 and two resistivity values were tried: 175 ohm-m, roughly the average reading obtained with the horizontal coplanar (HCP) coil orientation in 1979, and 700 ohm-m, the average for the vertical coplanar (VCP) orientation in 1979 (see App. A for explanation of these terms). Figure 11 shows that the 700-ohm-m value gives a very good fit, which implies that the dielectric and resistive values interpreted from these data represent no more than the top 3 m of ground. Higher resistivity values actually give shallower nulls in this case because the air and ground waves are not of the same amplitudes initially, as was seen in eq 4. At 88 MHz, 700 ohm-m gives an effective  $\kappa'' = 0.29$ .

The low frequency data are given in Figure 13. As at site 1, SI phase values in 1979 were predominantly above 45° whereas they were predominantly below 45° in 1980. This 1980 result contradicts the MI data which imply resistivity to be decreasing over the depth of penetration at 281 kHz. The low apparent resistivity values measured at 281 and 18.6 kHz for both years are, however, plausible at this site due to the lower resistivity of the first 6 to 7 m. The values  $\kappa' = 5.1$  and  $\rho = 700$  ohm-m give a skin depth at 88 MHz of about 8 m, which exceeds the depth that the value of 700 ohm-m represents. Therefore, as with

site 1, the ground refractive index must be continuously increasing with depth without any sharp electrical contrasts in order to produce data that allow a homogeneous interpretation.

### Site 3, marsh

The RFI profiles performed in 1979 and 1980 are given in Figures 14 and 15. The profiles in Figure 14 all show the characteristic  $1/y^2$  attenuation rate but only the one for 50 MHz shows any interference pattern. The first and only deep minimum at 50 MHz may be simulated theoretically with a homogeneous model of  $\kappa' = 5.1$  for any resistivity value  $> 10,000$  ohm-m, but the 1979 snow cover sufficiently attenuated the ground wave so that the air wave was mainly received.

Profiles were taken at several frequencies in 1980 but the only successful interference pattern obtained was at 80 MHz which is the solid trace shown in Figure 15. Profiles at lower frequencies were highly erratic and uninterpretable, while those at higher frequencies showed  $1/y^2$  attenuation as in Figure 14 without any ripples. The 80-MHz profile was not difficult to match theoretically and the resulting geologic interpretation is surprising but not implausible.

The geologic model shown in Figure 15 was developed as follows. The  $1/y^2$  attenuation rate and the fairly even spacing of the interference minima imply that only two guided modes propagated and that a good reflector existed at depth. The first try at interpretation assumed  $\kappa'_1 = 5.1$  (from Fig. 14),  $\tan \delta_1 = 0.0$  ( $\rho_1 = \infty$  ohm-m) and a reflection coefficient for the layer boundary of -1.0 (i.e.  $\rho_2 = 0.0$ ). After some trial and error, a model with  $\kappa'_1 = 5.5$  and a layer thickness of 1.37 m produced the correct spacing of minima and attenuation rate (dotted curve). This thickness is slightly greater than the depth at which the second mode begins to propagate.

In order to make depth of the minima decrease with distance, the second layer was given a finite resistivity of 1 ohm-m (dashed curve of Fig. 15). This made the two modes slightly leaky, with the one at a steeper angle of incidence with respect to the layer boundaries suffering the most leakage. The two guided modes for  $\rho_2 = 1$  ohm-m propagate at complex angles of  $27^\circ + i/0.019$  and  $61.8^\circ + i/0.009$ . The real parts of these angles vary insignificantly if the resistivity of the subsurface reflector is increased to 100 ohm-m, but the imaginary part steadily increases to give the modes greater attenuation. Both theoretical curves of Figure 15 vary little for  $\tan \delta_1 < 0.002$  so that  $\rho_1$  is probably greater than 25,000 ohm-m and therefore  $\kappa''_1 < 0.01$ .

An additional model was tried which assumed the lower layer to be a lossless dielectric having a lower dielectric constant than the upper layer. A value of  $\kappa'_2 = 3.5$  was chosen which would represent a layer of

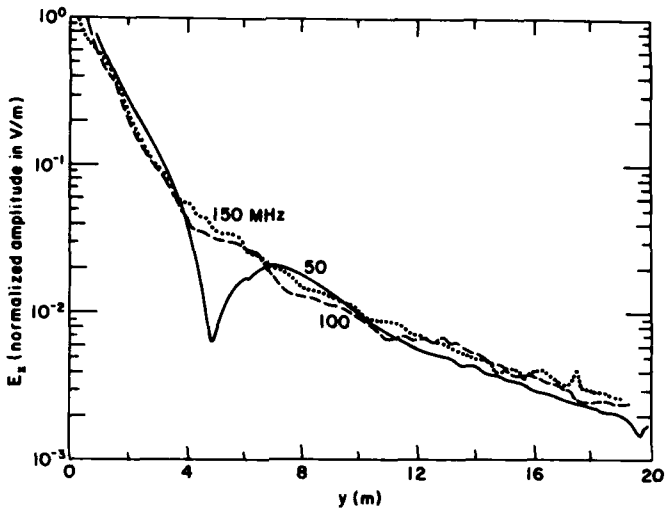


Figure 14. RFI profiles at three frequencies for April 1979 at site 3.

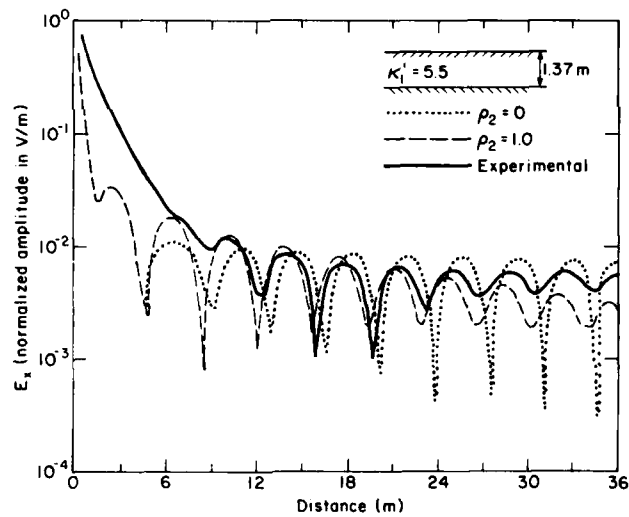


Figure 15. RFI profile at 88 MHz for April 1980 at site 3. Broken curves are generated by the ground models shown.

frozen sand or ice. The ratio  $\kappa'_2/\kappa'_1$  allows any mode incident at an angle greater than  $\sin^{-1}\sqrt{\kappa'_2/\kappa'_1}$  to propagate unattenuated. Therefore, since this angle =  $56^\circ$ , the mode at  $61^\circ$  propagated but the one at  $27^\circ$  was highly attenuated (the same layer depth was assumed). This strong attenuation of one mode occurs for any reasonable dielectric value and so no interference resulted.

Figure 16 shows the low frequency SI and MI data from 1979 and 1980. In 1979 all MI readings indicated resistivities greater than 10,000 ohm-m. In 1980, the VCP loop orientation readings indicated that resistivity was greater than 10,000 ohm-m, while the HCP loop orientation readings averaged around 3500 ohm-m over the section of the traverse containing the RFI profiles. As before, the SI resistivity values were much lower and

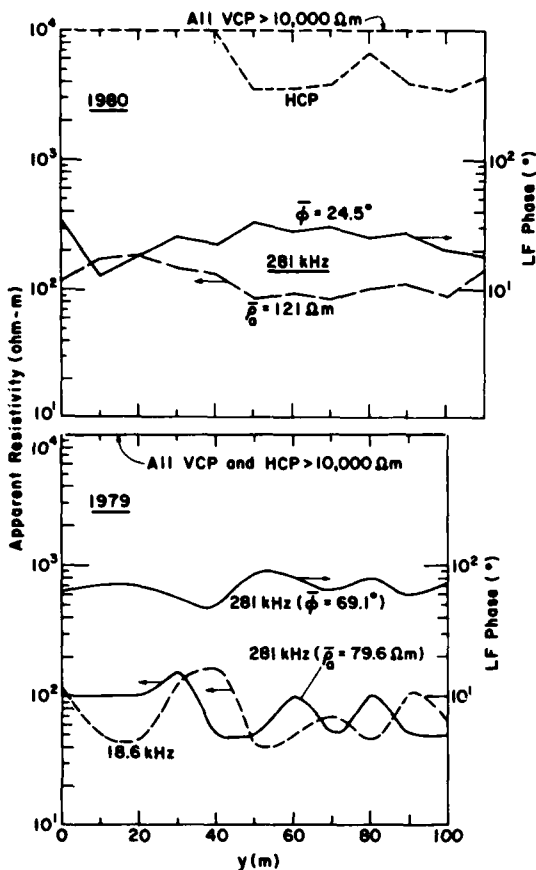


Figure 16. Magnetic induction and surface impedance data for site 3 during 1979 and 1980. Upper plots on each graph are magnetic induction readings in ohm-m of apparent resistivity. Arrows refer to applicable scales.

the implication of the phase data that resistivity decreases with depth was consistent with the MI readings only in 1979.

In order for the MI readings to remain quite high in the presence of a conductive layer, the layer must be quite thin. If we assume that the resistivity of the frozen silt is 25,000 ohm-m and the resistivity of the thin layer at 1.37-m depth is about 1 ohm-m, then the layer thickness must be only a few centimeters, so that the theoretical resistivity values of both the VCP and HCP configurations will be about 4500 ohm-m. This geologic model also gives SI values comparable to the 1979 data.

Unfortunately, no drilling was performed to validate the existence of a strong reflector within the first few meters. It is certain, however, that this is an unfrozen, brine layer, a phenomenon which occurs extensively throughout this area as discussed in the Pt. Barrow sites section. Therefore, it is not surprising that the SI measurements gave low resistivity

values as the LF and VLF radiowaves are sure to encounter brine-rich sediments.

## CONCLUSIONS

At site 1 (tundra, ice-rich silt)  $\kappa'$  was calculated at 4.0 and the resistivity at 4500 ohm-m for 50 MHz, which gives an effective  $\kappa'' \approx 0.08$ . At site 2 (beach ridge, ice-rich sand and gravel),  $\kappa'$  was calculated at 5.1 and the resistivity at 700 ohm-m for 88 MHz, which gives an effective  $\kappa' \approx 0.29$ . At site 3 (marsh, ice-rich silt),  $\kappa'$  was calculated at 5.1 (50 MHz) to 5.5 (80 MHz) and resistivity greater than 25,000 ohm-m (80 MHz) which gives an effective  $\kappa'' < 0.01$ . Since the resistivity values all agreed with those measured at 40 kHz using the magnetic induction method, dielectric loss was due to d.c. effects and not relaxation processes. In many cases, the lack of an interference pattern at VHF suggested very low resistivity, but this was explained by the attenuation of the inhomogeneous air wave due to the snow cover.

The RFI technique seemed to evaluate the electrical properties of only the upper few meters of ground, as was most obvious at site 3. The positive conductivity gradient with depth at sites 1 and 2 most likely caused the subsurface wavefront normals to refract downwards with an associated attenuation in the field strength. This attenuation made inhomogeneous ground (as evidenced by the LF data) appear homogeneous for the majority of traverses because no sharp interfaces existed at sites 1 and 2.

The data obtained on dielectric properties may be compared with previous laboratory investigations of silt. As mentioned in the *Introduction*, Hoekstra and Delaney (1974) measured the dielectric constant of several dry materials (fine sand, silt, clay) at 500 MHz and found all materials to have  $\kappa'$  values of approximately 3 within a few percent. Since ice has a  $\kappa' = 3.2$ , we must therefore conclude that either the organic material present at Pt. Barrow or a small amount of unfrozen water adsorbed on the soil particles is responsible for raising the observed values of  $\kappa'$  to 4.0 to 5.5 (sites 1 and 3), measured to an accuracy of about  $\pm 3\%$ . Our opinion is that the unfrozen, adsorbed water is responsible for elevating the dielectric constant, although we have no data as to the effect of the organic content. This opinion is based on laboratory time domain reflectometry (TDR) measurements by one of us (A. Delaney) on an organic silt at a water content of 1.8 g H<sub>2</sub>O/g silt (180% water by weight) between 10 and 1000 MHz. For frequencies below 1000 MHz,  $\kappa'$  varied between 5.5 and 6.0 at temperatures below -15°C which was near the ground surface temperatures at Pt. Barrow.  $\kappa'$  then slowly increased as temperature and therefore unfrozen water increased.

The dielectric constant of 5.1 determined for the sandy gravel at site 2 is unexpectedly high in view of the cold ground temperatures, the decrease in available surface area for adsorbed water (relative to the silt), and the  $\kappa'$  values for dry sands and gravels of about 3. However, the low frequency resistivity was also unusually low, probably due to the higher-than-usual salt concentrations that exist near or at the surface of this raised beach ridge. The high salt concentration is documented in the report of Brown (1969) who has shown that heavier salt concentrations occur nearer the surface (within about 1 m) of the beach ridges than of the tundra or marsh flats. Therefore, it is the elevated salt concentrations that probably raised  $\kappa'$  of the sand and gravels above that of the silts. In non-marine environments, frozen sands or gravels will probably exhibit  $\kappa'$  values between 3 and 4.

The difference in dielectric values between the tundra and the marsh sites may result from a greater proportion of finer grain sediments existing in the marsh but this is not known. At the marsh site the two-layer interference pattern implied a resistivity of at least 25,000 ohm-m, whereas the homogeneous interference pattern at the tundra site gave a value of about 4500 ohm-m. The discrepancy in these resistivity values draws us to the conclusion that the tundra site value is probably too low, again due to snow cover attenuation of the inhomogeneous air wave. At the marsh site, snow cover would also affect the strength of the inhomogeneous modes, but both modes would be similarly affected so that the interference pattern would remain intact. The ratio of the mode amplitude would change by only 25% for a 20-cm snow cover, whereas at site 1 the ratio of the air wave amplitude to that of the inhomogeneous wave would change by 52%. Therefore we believe that resistivity values of the first few meters were in excess of 25,000 ohm-m at both sites 1 and 2.

## LITERATURE CITED

Annan, A.P. (1973) Radio interferometry depth sounding: Part I—theoretical discussion. *Geophysics*, vol. 38, no. 3, p. 557-580.

Annan, A.P. (1976) Density of ice samples from "Involute Hill" test site, District of Mackenzie: Report of activities, Part C. *Geologic Survey of Canada, Paper 76-1C*, p. 91-95.

Annan, A.P. and J.L. Davis (1976) Impulse radar sounding in permafrost. *Radio Science*, vol. 11, no. 4, p. 383-394.

Arcone, S.A. (1979) A review of electrical resistivity of frozen ground and some electromagnetic methods for its measurement. *Materials Performance*, vol. 18, no. 5, p. 32-37.

Arcone, S.A., P.V. Sellmann and A.J. Delaney (1979) Effects of seasonal changes and ground ice on electromagnetic surveys of permafrost. *CRREL Report 79-23*. ADA 077903.

Arcone, S.A. and A.J. Delaney (1980) Low frequency surface impedance measurements at some glacial areas in the United States. *Radio Science*, vol. 15, no. 1, p. 1-9.

Black, R.F. (1964) Gubic formation of Quaternary age in northern Alaska. In *Exploration of Naval Petroleum Reserve No. 4, 1944-1953*. U.S. Geological Survey Professional Paper 302-C, Part 2, p. 59-91.

Brown, J. (1969) Ionic concentration gradients in permafrost in Barrow, Alaska. *CRREL Research Report 272*. AD 699329.

Brown, J. and P.L. Johnson (1965) Pedo-ecological investigations—Barrow, Alaska. *CRREL Technical Report 159*. AD 615998.

Budden, K.G. (1961) *The wave-guide mode theory of wave propagation*. Englewood Cliffs, N.J.: Prentice Hall, Inc.

Cook, J.C. (1960) RF electrical properties of salty ice and frozen earth. *Journal of Geophysical Research*, vol. 65, no. 6, p. 1767-1771.

Davis, J.L., W.F. Scott, R.M. Morey and A.P. Annan (1976) Impulse radar experiments on permafrost near Tuktoyaktuk, Northwest Territories. *Canadian Journal of Earth Science*, vol. 13, no. 11, p. 1584-1590.

Gold, L.W. and A.H. Lachenbruch (1973) Thermal conditions in permafrost—A review of North American literature. In *Permafrost: North American Contribution to the Second International Conference*, Yakutsk. Washington, D.C.: National Academy of Sciences.

Hasted, J.B. (1973) *Aqueous dielectrics*. London: Chapman and Hall.

Hoekstra, P. and W. Doyle (1971) Dielectric relaxation of surface adsorbed water. *Journal of Colloid and Interface Science*, vol. 36, no. 4, p. 513-521.

Hoekstra, P. and A. Delaney (1974) Dielectric properties of soils at UHF and microwave frequencies. *Journal of Geophysical Research*, vol. 79, no. 11, p. 1699-1708.

Katsube, T.J., M. Wadleigh and R. Erickson (1976) Electrical properties of permafrost samples: Report of activities. *Geologic Survey of Canada, Paper 76-1C*, Part C, p. 83-90.

Keller, G.V. and F.C. Frischknecht (1966) *Electrical methods in geophysical prospecting*. New York: Pergamon Press.

Norton, K.A. (1937) The propagation of radio waves over the surface of the earth and in the upper atmosphere. Part I. *Proceedings, Institute of Radio Engineers*, vol. 24, p. 1367-1387. Part II. *Proceedings, Institute of Radio Engineers*, vol. 25, p. 1203-1236.

Olhoeft, G.R. (1977) Electrical properties of natural clay permafrost. *Canadian Journal of Earth Sciences*, vol. 14, no. 1, p. 16-24.

O'Sullivan, J.B. (1963) Geochemistry of permafrost: Barrow, Alaska. In *Proceedings, Permafrost: International Conference*, Lafayette, Indiana.

Rossiter, J.R., G.A. LaTorreca, A.P. Annan, D.W. Strangway and G. Simmons (1973) Radio interferometry depth sounding. Part II: Experimental results. *Geophysics*, vol. 38, no. 3, p. 581-599.

Rossiter, J.R., D.W. Strangway, G. Koziar, J. Wong and G.R. Olhoeft (1978) Electromagnetic sounding of permafrost, N.W.T., Canada, in summer and winter. In *Proceedings of the Third International Conference on Permafrost, July 10-13, 1978, Edmonton, Alberta, Canada*. Ottawa: National Research Council of Canada.

Sellmann, P.V. and J. Brown (1973) Stratigraphy and diagenesis of perennially frozen sediments in the Barrow, Alaska, region. In *Permafrost: North American Contribution to the Second International Conference*. Washington, D.C.: National Academy of Sciences, p. 171-181.

Sinha, A.K. (1976) Determination of ground constants of permafrost terrains by an electromagnetic method. *Canadian Journal of Earth Sciences*, vol. 13, p. 429.

Strangway, D.W. (1969) Moon electrical properties of the uppermost layers. *Science*, vol. 65, p. 1012-1013.

Strangway, D.W., G. Simmons, G. LaTorreca, R. Watts, L. Bannister, R. Baker, J.D. Redman and J.R. Rossiter (1974) Radio-frequency interferometry—a new technique for studying glaciers. *Journal of Glaciology*, vol. 13, p. 123-132.

Sommerfeld, A. (1909) Über die Ausbreitung der Wellen in der drahtlosen Telegraphie. *Annalen der Physik*, vol. 28, p. 665-737.

Von Hippel, A. (1954) *Dielectrics and waves*. Cambridge, Mass.: M.I.T. Press.

Wait, J.R. (1951) The magnetic dipole over the horizontally stratified earth. *Canadian Journal of Physics*, vol. 29, p. 577-592.

Wait, J.R. (1970) *Electromagnetic waves in stratified media*. New York: Pergamon Press, 2nd edition.

Wong, J., J.R. Rossiter, G.R. Olhoeft and D.W. Strangway (1977) Permafrost: electrical properties of the active layer measured in situ. *Canadian Journal of Earth Sciences*, vol. 14, no. 4 (Part 1), p. 582-586.

## APPENDIX A: DISCUSSION OF LOW-FREQUENCY GEOPHYSICAL METHODS

### Surface impedance

The surface impedance method utilizes the electromagnetic field components of a ground or sky wave propagating from a distant or local transmitter to measure earth resistivity and estimate the layering involved. At low frequencies, vertical monopole antennas are used in the VLF (3 to 30 kHz) and LF (30 to 300 kHz) bands. These antennas radiate vertically polarized waves that contain three field components at the earth's surface: a vertical electric field  $E_z$ , a radial electric field  $E_r$ , and an azimuthal magnetic field  $H_\phi$ . The quantity of interest is the complex surface impedance  $Z_s$  defined as

$$Z_s \text{ (ohms)} = E_r / H_\phi \Big|_{z=0} \quad (A1)$$

from which ground resistivity variations may be interpreted, especially if signals at several different frequencies are available. Displacement currents are usually neglected in comparison with conduction currents at these low frequencies.

The complex quantity  $Z_s$  is usually expressed as a modulus  $M$  and a phase  $\psi$  by

$$Z_s = M e^{i\psi}. \quad (A2)$$

This quantity is easily derived for a vertically stratified earth model of any number of layers (e.g. Wait 1970). For a homogeneous model of resistivity  $\rho$ ,  $M$  is found to be  $\sqrt{\omega\mu_0\rho}$  and  $\psi = 45^\circ$ . In general, an apparent resistivity  $\rho_a$  is defined such that

$$\rho_a = M^2 / \omega\mu_0. \quad (A3)$$

Phase usually indicates the nature of the stratification. Phase values greater than  $45^\circ$  generally mean that resistivity *decreases* with depth, while values of less than  $45^\circ$  generally mean that resistivity *increases* with depth. The depth to which readings are significant depends on the resistivities and thicknesses of the individual layers. If a significant change in resistivity occurs below the skin depth  $\delta$  of a material where

$$\delta = \sqrt{2\rho/\omega\mu_0}, \quad (A4)$$

then the material beneath that interface will have little effect on  $Z_s$ .

For these studies a Geonics EM-32 surface impedance unit was used to monitor an LF transmitter operating at

Pt. Barrow at 281 kHz. A Geonics EM-16R unit was used to monitor a VLF transmitter operating north of Seattle, Washington, at 18.6 kHz. Both instruments use a small ferrite-loaded coil to measure  $H_\phi$  and two ground probes to measure  $E_r$ . The ground probes for the EM-32 are spaced 2 m apart and for the EM-16R they are 10 m apart.

### Magnetic induction

The magnetic induction method derives ground resistivity values from the amount of magnetic field coupling between two loop antennas located at or slightly above the earth's surface. One loop, the transmitter, generates a primary a.c. magnetic field  $H_p$  that couples directly to the receiver loop through free space and also induces eddy currents within the earth. These currents then regenerate a secondary magnetic field  $H_s$  which also couples with the receiver. The ratio  $H_s/H_p$  depends on ground resistivity but is also affected by loop separation and orientation, loop height above ground, and transmitter frequency. The quantity usually measured is the mutual impedance  $Z$  which is often normalized by the mutual impedance  $Z_0$  for loops situated in free space. The mutual impedance  $Z$  is defined as  $V/I$  where  $V$  is the voltage induced in the receiver loop and  $I$  is the current in the transmitter loop.

At very low frequencies and below, the normalized mutual impedance  $Z/Z_0$  for two horizontal coplanar loop antennas upon a homogeneous model earth can be well approximated from an expression found in Keller and Frischknecht (1966) by the formula

$$Z/Z_0 = (kr/2)^2 \quad (A5)$$

where  $k = \sqrt{i\omega\mu_0/\rho}$  and  $r$  is the transmitter-receiver separation. Most often it is the imaginary or phase quadrature component of  $Z/Z_0$  that is measured because of its greater range of linearity with respect to resistivity. When the earth is layered, an apparent resistivity must then be defined which corresponds to the equivalent resistivity that would produce the same mutual impedance above a homogeneous earth. Interpolation curves or computational integrations of integral equations (e.g. Sinha 1976) must then be used to resolve the different layer resistivities and thicknesses.

In practice, the transmitter and receiver loop antennas may be oriented horizontally (HCP) or vertically (VCP) coplanar, or even coaxially. In these studies the coplanar orientations have been used with the commer-

cially available Geonics EM-31. The device we used operated at 40 kHz, a frequency at which the depth of sensitivity depends primarily on  $r$  and is independent of ground resistivity. In this case,  $r$  is 3.66 m, allowing a depth of exploration of approximately 7 m when the antenna loops are HCP and about 3 m when they are VCP.

A facsimile catalog card in Library of Congress MARC format is reproduced below.

Arcone, Steven A.

VHF electrical properties of frozen ground near Point Barrow, Alaska / by Steven A. Arcone and Allan J. Delaney. Hanover, N.H.: U.S. Army Cold Regions Research and Engineering Laboratory; Springfield, Va.: available from National Technical Information Service, 1981.

iv, 21 p., illus., 28 cm. ( CRREL Report 81-13 )  
Prepared for Directorate of Military Programs-  
Office of the Chief of Engineers by Corps of Engineers, U.S. Army Cold Regions Research and Engineering Laboratory under DA Project 4A161102AT24.

Bibliography: p. 14.

1. Dielectric properties. 2. Permafrost. 3. Point Barrow, Alaska. 4. Radio interferometry. I. Delaney, Allan J. II. United States. Army. Corps of Engineers. III. Cold Regions Research and Engineering Laboratory. IV. Series: CRREL Report 81-13.

DATE  
ILMED  
-8